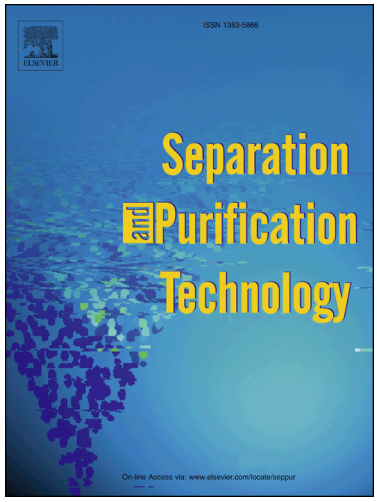

Inferring In-situ Floc Size, Predicting Solids Recovery, and Scaling-up using the Leung Number in separating Flocculated Suspension in Decanter Centrifuges

Wallace Woon-Fong Leung

PII: S1383-5866(16)31018-8
DOI: http://dx.doi.org/10.1016/j.seppur.2016.07.010
Reference: SEPPUR 13127

To appear in: *Separation and Purification Technology*

Received Date: 31 March 2016
Revised Date: 26 May 2016
Accepted Date: 12 July 2016

Please cite this article as: W.W-F. Leung, Inferring In-situ Floc Size, Predicting Solids Recovery, and Scaling-up using the Leung Number in separating Flocculated Suspension in Decanter Centrifuges, *Separation and Purification Technology* (2016), doi: http://dx.doi.org/10.1016/j.seppur.2016.07.010

Inferring In-situ Floc Size, Predicting Solids Recovery, and Scaling-up using the Leung Number in separating Flocculated Suspension in Decanter Centrifuges

Wallace Woon-Fong Leung

Mechanical Engineering, The Hong Kong Polytechnic University, Hung Hom, Hong Kong

Abstract

Centrifugation accompanied by flocculation of fine biosolids is often utilized in wastewater treatment. Unfortunately, commonly used laboratory jar tests often over-estimate the size of the flocculated solids (flocs) that can be realized in-situ in the centrifuge as the fragile flocs can be easily broken by shear and turbulence during feed acceleration in the centrifuge. Currently, there is no satisfactory method to predict in-situ floc size in the centrifuge, despite the floc size is critical to separation and solids recovery. The difficulty in making predictions also leads to inaccuracy in predicting solids recovery by decanter centrifuge and scale-up between centrifuges of different sizes, designs, and operating conditions, which is an even more serious issue. This study attempts to address these hurdles.

In this study, first the flow pattern in a decanter centrifuge in form of moving layer at the pool surface is demonstrated by two different experiments. Second, a model on separation of suspended flocs in the moving layer in a centrifuge is developed. Further, a two-parameter model is proposed to represent the floc size distribution wherein the first parameter represents the minimum floc size (primary particle without coagulation or flocculation) and the second parameter represents

the median floc size. A closed form analytical solution for the model is obtained with results expressed in a dimensionless Leung number and the ratio of minimum-to-median floc size. Third, a Buckingham-π analysis has been conducted on separation in a moving layer under centrifugal field confirming these two governing dimensionless parameters can also be derived from the more basic dimensionless π groups. Fourth, by matching the solids recovery obtained from field tests with the model prediction, the median floc size can be inferred. In this matching process, the minimum floc size is assumed to be equal to the size of the primary, unflocculated solids. Fifth, four sets of tests (over 20 runs) have been carried out using two decanter centrifuges of different sizes and designs operating, respectively, under different pool depths, feed rates, polymer dosages and rotation speeds in a wastewater treatment plant processing mixed sludge with 48% primary sludge and 52% waste activated sludge. The median floc size inferred from the present method is in the range of 4 to 9 mm from the three series of tests (14 tests). The improved feed acceleration design with speed matching closely that of the rotating pool results in less pool turbulence, larger flocs, and lower polymer dosage (7 kg polymer/ton sludge); while the poorer feed acceleration with more pool disturbance from the under-accelerated feed results in smaller flocs, and higher polymer dosage (9 kg/t). Sixth, an important application of the model is to predict solids recovery using an estimated median floc size and this approach has predicted the solids recovery reasonably well on the fourth set of tests (9 tests). Seventh, the scale-up for predicting solids recovery of flocculated suspension from decanter centrifuges of

different sizes, designs, and operating conditions has been demonstrated using the dimensionless Leung number and the floc minimum-to-median size ratio.

Keywords: flocculated suspensions, in-situ floc size, decanter centrifuge, solids recovery, Leung number, wastewater treatment, model, field testing

1. Introduction

1.1 Coagulation and Flocculation

In processing biological solids such as municipal and industrial wastewater sludges, the solids are very fine from micron to submicron ranges and the density difference between the solids and the suspending medium is very small, both of which results in difficult separation. Coagulants, such as aluminum sulfate, ferric chloride and ferric sulfate, are used to neutralize the charges (typically negative) left on the particles that keep them in dispersion by electrical repulsion in a suspension. Upon being neutralized, the particles can agglomerate to larger particles by the Van der Waals' attractive force. Another effective solution to separate these fine particles is to flocculate the suspension with polymers which can extend their molecular chain in solution attracting and wrapping up the smaller particles by ionic or non-ionic interactions (Van der Waals' force) such that much larger stable flocculated particles form that can settle readily under centrifugation [1-3]. The polymer (also known as polyelectrolytes) used for flocculation can be anionic or cationic to neutralize the charges left on these fine particles in the flocculation process to form much larger flocculated solids

(abbreviated as floc). Both coagulation and flocculation can work independently, or in combination, to achieve the most desirable results.

1.2 Decanter Centrifuge

A decanter centrifuge [4, 5] is predominantly horizontally mounted and has a rotating bowl and a rotating conveyor screw, see sectional view of a decanter in Fig. 1a. Both the bowl and the conveyor screw rotate at high angular speed to produce an equivalent acceleration of 2000-3500g (1 g = 9.81 m/s^2); however, there is a small differential speed between these two components that is responsible for conveying the sediment or cake. In Fig. 1a, slurry is fed into the decanter through a stationary feed pipe. The feed slurry picks up tangential speed when it is in contact with the feed accelerator installed in the rotating conveyor hub. After the feed leaves the feed port of the accelerator at radius R_a, it is dropped (free-flight) onto the surface of the rotating liquid pool at radius R_p. In the pool, under centrifugal acceleration heavier solids settle to the inner wall of the bowl to form a cake. The differential rotation between the conveyor and bowl drives the cake up the conical beach and out of the machine. During cake transport, under centrifugal acceleration additional liquid is being expressed out of the cake back into the pool. The clarified effluent, free from solids, overflows at the centrate end of the machine, see Fig. 1a.

For biosolids waste applications, polymer or flocculent with concentration 0.1% - 0.3% is added to the feed prior to the feed slurry entering the machine. At times, polymer may be fed through a dedicated pipe into the feed compartment for

which the feed and polymer are mixed energetically before discharging out of the feed ports to the pool.

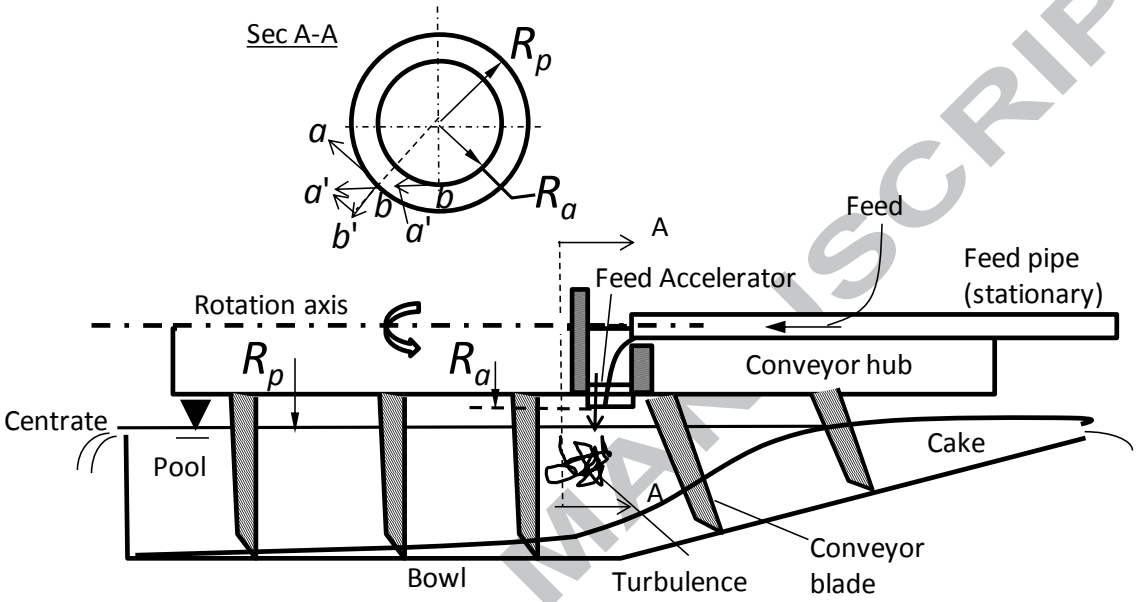

Fig. 1a – Schematic of a decanter with inset showing section A-A through the feed location to the pool. Other than the feed pipe, all the components are rotating. The ***ba', b'a', bb', and ba*** represent velocity vectors in the inset of the figure.

1.3 Problems

Jar tests [1, 6] are commonly used in the laboratory wherein the feed sludge from the plant is tested against different polymers or flocculants to identify which flocculant can provide a large stable floc after subjecting to intense mixing for a period of time. This is important especially with feed that varies in properties daily, if not hourly, in the wastewater treatment plant. Of course, different types of flocculants, different dosages as well as different concentrations from the same

polymer can be tested. Unfortunately, this represents only a very “crude” or “rough” test as the in-situ floc size and characteristics in the separation pool of the centrifuge may be very much different from those that have been realized from the laboratory jar test. The jar test takes place in a “calm” environment in the absence of flow dynamics, therefore it cannot reproduce the in-situ test environment of the floc in the separation pool, which can be subject to extremely high shear from turbulence in the pool. It has long been known that turbulence can break-up flocs [7]. Turbulence is induced when the feed enters the rotating pool in the centrifuge with a velocity (including both tangential and radial components) that differs from that of the pool [4]. Two cantilever bowls with the front end open up for flow visualization has been setup to qualify and quantify feed velocity mismatch with that of the rotating pool [8]. One setup has the improved feed accelerator equipped with overspeeding vanes and smoothener [9-10] that facilitated feed entering the rotating pool at the matched tangential speed of the pool. The other setup has a conventional feed accelerator that has two open ports in the hub at a smaller radius resulting in poor feed acceleration from the radial drop of the feed onto the pool surface at a larger radius. As such, the feed velocity is much below that of the rotating liquid pool. Using a stroboscope, turbulence was observed on the pool surface [10] with the conventional feed accelerator especially at higher feed rate, while the pool surface was smooth (almost having a mirror-finish surface) and calm [10] with the improved feed accelerator that has equipped with the overspeeding vanes and a smoothener [9]. Measurements on feed efficiency at the pool surface have also

been carried out using a pool meter for both of these setups as a function of different feed rates [4, 8]. The results confirmed that a significant loss in acceleration efficiency due to turbulence at the pool with conventional feed accelerator especially at high feed rate, while the efficiency was nearly 100% for the calm smooth pool fed with the improved feed accelerator.

A common problem associated with practically all conventional feed accelerator designs is that there is a radial drop of the feed onto the pool resulting in acceleration inefficiency, turbulence and mixing [4, 9]. In section A-A in Fig. 1a, suppose the feed slurry is accelerated to solid-body rotation with tangential speed V_t represented by the vector ***ba'*** at the accelerator discharge port radius R_a, i.e. $V_t=\Omega R_a$, where Ω is the angular speed of the accelerator. As the feed lands onto the pool at a larger radius R_p after free-flight from the accelerator, the tangential component is reduced to vector ***b'a'*** [= ***ba'*** (R_a/R_p)] as a result of conservation of moment of momentum [4]. Therefore, vector ***b'a'*** is much reduced when compared to the tangential pool speed at solid-body rotation, $V_p=\Omega R_p$, represented by the vector ***ba***. In addition, a new radial velocity component vector ***bb'*** is induced that sends the feed plunging into the pool in the radial direction. Both mismatch in tangential speed and a significant radial velocity result in shear and turbulence breaking up delicate, large flocs to smaller sizes.

Another problem is the large variability of feed properties, such as those found in municipal wastewater, which vary daily if not hourly; therefore, it is difficult to predict the settling behavior of the flocculated feed slurry and thus the solids

recovery in a decanter centrifuge. Further, a common yet serious issue is to scale-up from a small to a large sized decanter centrifuge.

The problems on uncertainty of the floc size, performance prediction or projection, and machine scale-up are indeed inter-related, and all these issues will be addressed in the present investigation.

2. Our Work

In this work, first two experiments with results will be presented on the establishment of the moving layer in a centrifuge with an annular pool. The results are applicable to both the decanter and tubular centrifuges. Next, a model is presented on sedimentation of flocculated suspension with a floc size distribution, which is based on two sizes, the minimum size (i.e. the basic primary particles in the sludge before agglomeration) and the median size. The separation of the flocs is assumed to take place in a thin moving layer. The problem is solved analytically (confirmed also numerically) and the solids capture, or solids recovery, is expressed as function of a dimensionless Leung number, *Le*, and a dimensionless minimum floc size, $\overline{x_o}$. These are defined in Eqs. 9 and 11, respectively, in the text to follow.

Extensive field tests have been carried out in a wastewater treatment plant on mixed sludge and solids recovery data have been collected for two decanter centrifuges running side-by-side. One machine was operated with changing parameters while the operating parameters of the second machine were held

constant to compensate for variability of municipal sludge especially during summer. Four sets of tests, encompassing over 20 individual tests, have been conducted collectively on the two decanter centrifuges under different feed rates, pool levels, polymer dosages, and rotation speeds. Three sets of tests (over 14 runs) have been used with the present model to infer the in-situ median floc size and the minimum floc size was taken as the size corresponding to the unflocculated primary particle in the sludge. The determined in-situ floc sizes were in agreement with the acceleration efficiency of the two machines from their design and operating pool levels, as well as the actual polymer consumption of the two machines in the tests. Further, the model was used to predict the fourth set of test results (9 runs) with reasonably good agreement. Finally, the Leung number was used to scale-up all the test results obtained from the two decanter centrifuges operating at different conditions.

2.1 Observation of Moving Layer

In our laboratory, two experiments have been carried out to visualize the moving layer containing the incoming feed slurry in the decanter. In the first experiment, the feed water was introduced to fill a bowl 267-mm diameter rotating at 970 rev/min. Water was allowed to overflow at the opposite end of the bowl from the feed end through a set of ring weirs. After steady state has been reached, the feed to the pool was changed to another source with water mixed with fluorescent dye. The room light was turned off and an ultraviolet light source was used to illuminate the pool surface. The moving layer was observed as a

fluorescent thin ring of fluid located at the pool surface, which rested on an otherwise stagnant fluid pool in the bowl. The stagnant fluid was the initial water pool (appeared dark) that did not contain the fluorescent dye. This is shown in Fig. 1b. In order to obtain a good image of the pool, instead of shooting at dead center along the axis of rotation, a better image was taken with the camera slightly tilted at an oblige angle to the axis showing a moving layer, thicker than the actual value, resting on an otherwise stagnant pool.

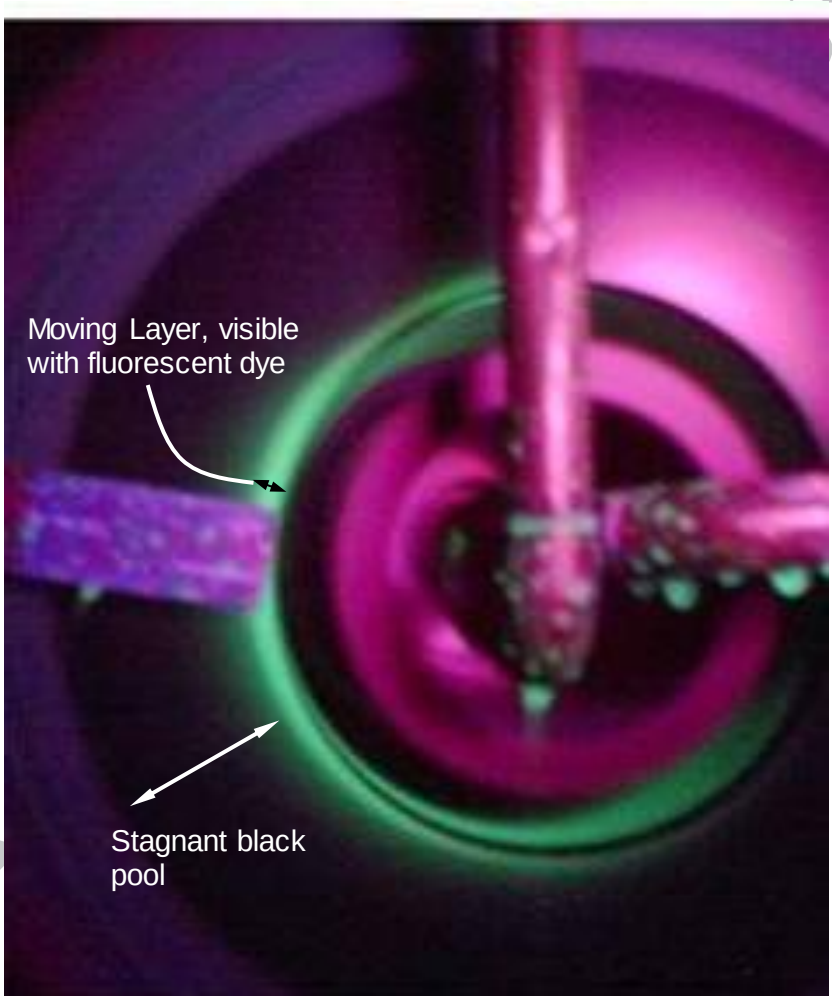

Fig. 1b –Fluorescent dye indicated the presence of the moving layer at the pool surface. Given the angle of the camera the moving layer appeared to be thicker than it should.

The actual moving layer (bright ring) was of order of 1 mm. Below the moving layer was a thick stagnant pool (dark).

In another test, the bowl with the same rotating speed was filled initially with water that was acidic. After the bowl was completely filled with acidic water, the feed was switched to plain water. Immediately (at time zero), the effluent was collected and the conductivity of the effluent water was measured during the switch-over. Instead of measuring time, the number of pool volumes was used to replace time, which is equivalent to measuring time given the pool volume was fixed by the overflow weir and the feed rate was fixed at 221 mL/s during the entire experiment. The results are presented in Fig. 1c. As shown in Fig. 1c, the normalized conductivity started at 1.8 and decreased to practically zero after two pool volumes. Subsequently, it was maintained zero until a total of 30 pool volumes have been fed through the bowl at which the feed was stopped abruptly and the machine was shut down. During shut down, the pool collapsed when the centrifugal field dropped below a critical level to maintain solid-body rotation and the conductivity of the effluent rose abruptly to 0.6, see Fig. 1b. This indicates that the stagnant pool was acidic and it did not interact with the feed in the moving layer until the pool has collapsed. As such, these two definitive experiments clearly pin-point the presence of the thin moving layer riding on top of an inactive (flow-wise) stagnant pool.

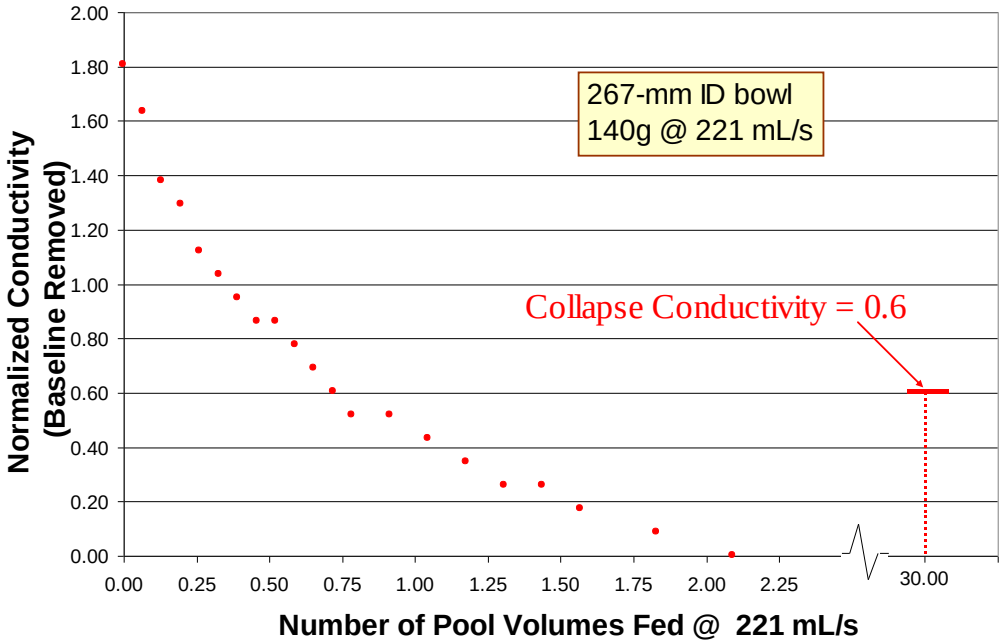

Fig. 1c – Normalized conductivity versus pool volume of water feed to the rotating bowl.

2.2 Moving Layer Model

It has been shown in sec. 2.1 that the feed flows across the centrifuge clarifier in a thin moving layer, which rests on an otherwise quiescent stagnant clarifier pool of liquid. This is especially when the feed is not fully accelerated. This is depicted in Fig. 2. The flocs settle across the layer as they move with the flow across the clarifier from the feed introduction to the effluent exit. Below the moving layer is a quiescent zone where fluid flow is relatively slow except at the end walls perpendicular to the bowl wall with thin Ekman boundary layers [4]. In this quiescent zone, flocs settle toward the bowl wall forming a sediment or cake layer, which is being transported by the screw conveyor toward the beach and out of the bowl. Therefore, it is critical for the flocs to settle in the moving layer to ensure being separated in the centrifuge.

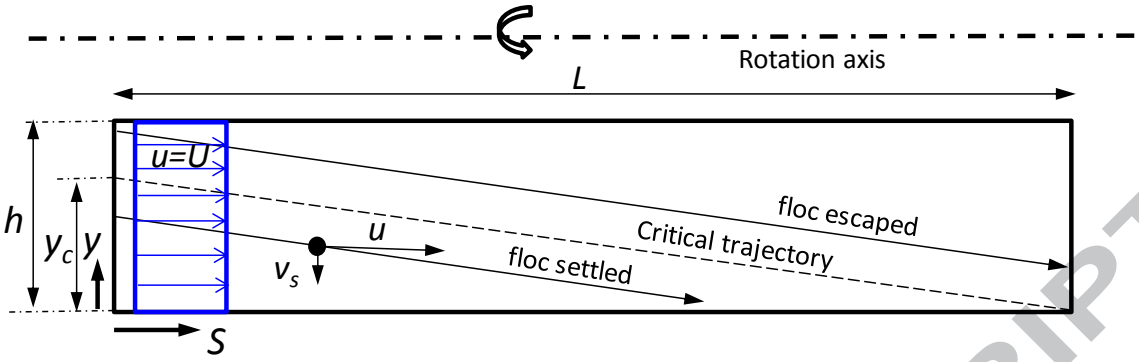

Fig. 2 – Settling in the thin moving layer. (The thick stagnant quiescent pool layer below the moving layer is not shown.) The black dot represents the floc being subject to both throughflow and transverse velocities. The broken-line path represents the critical trajectory where the floc just settles after being transport across the clarifier. The path below the critical trajectory with $y(S=0) < y_c$ represents that the floc would have settled in the moving layer, whereas the path above the critical trajectory with $y(S=0) > y_c$ represents the floc would have escaped from settling in the clarifier. (Note schematic is not to scale)

Consider a floc with equivalent diameter x (i.e. volume of the sphere with diameter x being identical to that of actual floc volume) that settles in the moving layer with thickness h. As shown in Fig. 2, the floc is subject to both the throughflow velocity $u=U$ along the axis S affixed in the flow direction along the clarifier, and the Stokes' settling velocity v_s directed toward the clarifier bowl wall in the radial direction. v_s is given by the Stokes' law on settling modified by the centrifugal acceleration from 1g,

$$v_s = \frac{1}{18}\frac{(\Delta\rho/\rho)Gx^2}{\mu} \qquad (1a, b)$$

$$G = \Omega^2 R_p$$

As both longitudinal and transverse velocities are constant, therefore the floc travels in a linear trajectory in the moving layer as depicted in Fig. 2. Also, given the moving layer is relatively thin (see Fig. 1b) the entire moving layer has practically the same radius corresponding to the pool surface radius R_p. An important assumption in this model is that flocs of all sizes are uniformly distributed across the moving layer of thickness h at the inlet. Consider the floc with equivalent diameter x being located initially at the feed inlet S=0 at y=y_c with the y-axis directed towards the rotation axis of the clarifier, see Fig. 2. It is such that as the floc travels to the effluent end of the clarifier it just settles out of the moving layer; and this path taken by the floc corresponds to the limiting trajectory. Therefore, a floc at an initial position $y \le y_c$ settles out of the moving layer; vice versa when the floc is at initial position $y > y_c$ the floc escapes without sedimenting in the moving layer. It follows that the capture efficiency, $z(x)$, for a floc with diameter x is given by

$$z(x) = \frac{y_c}{h} \qquad (2a)$$

The limiting trajectory can be determined from the retention time t_R

$$t_R = \frac{L}{u} = \frac{y_c}{v_s} \qquad (3)$$

Note L is the claifier length of the decanter. By continuity,

$$u = \frac{Q}{2\pi R_p h} \tag{4}$$

It has been assumed that the moving layer thickness *h* being so thin that the cross sectional area can be approximated by the annular area, $2\pi R_p h$.

Using Eqs. 1, 3, and 4, Eq. 2a can be expressed as,

$$z(x) = \left(\frac{x}{x_c}\right)^2, \quad x \le x_c$$

$$z = 1, \quad x > x_c \tag{2b, c, d}$$

$$x_c = \sqrt{\frac{9Q\nu}{\pi R_p LG(\Delta\rho/\rho)}}$$

ν is the kinematic viscosity of the suspension μ/ρ. x_c is the cut size which corresponds to the smallest floc size that can be settled completely in the moving layer. It is clear from Eq. 2b that the capture rate by sedimentation varies as the second power of the floc size, *x,* as a consequence of the Stokes' law. When $x=x_c$, $z=1$.

Assuming the flocs have a particle size distribution (PSD) that can be expressed by the cumulative undersize, *F(x),* and the frequency density distribution, *f(x)*. These two quantities are related by,

$$F(x) = \int_0^x f(x)dx \tag{5a, b}$$

$$f = \frac{dF}{dx}$$

The solids recovered by separation is $z(x)f(x)dx$. Thus, the total solids recovery R_s is given by summing up all the possible settleable particle sizes,

$$R_s = \int_0^\infty z(x)\, f(x)dx = \int_0^\infty z(x)dF = \int_0^{x_c} z(x)dF + 1 - F(x_c) \qquad (6)$$

Note this relationship is very general without making any assumption on the specific form on the feed floc PSD. For a given PSD, Eq. 6 can be easily integrated numerically.

2.2 Feed Profile

Suppose the PSD of the flocs is given by a two-parameter correlation with the two parameters a and x_o as given below,

$$F(x) = \exp(a[x - x_o]) - 1, \quad x \le x_{\max}$$
$$F(x) = 1, \quad x > x_{\max} \qquad (7a, b)$$

From the distribution, the maximum size x_{max} and median size $x_{50\%}$ can be readily determined by setting F=1 at x=x_{max} and F=0.5 at x=$x_{50\%}$,

$$x_{\max} = x_o + \frac{\ln 2}{a} = x_o + \frac{0.693}{a}$$
$$x_{50\%} = x_o + \frac{\ln(3/2)}{a} = x_o + \frac{0.405}{a} \qquad (7c, d)$$

Note x_o corresponds to the minimum floc size, which is the primary sludge particle without flocculation and coagulation. For a given x_o, either a, x_{max} or $x_{50\%}$, determines the entire PSD. It is most appropriate to choose the median floc size $x_{50\%}$. By way of example, Fig. 3a shows three feed floc distribution profiles with

$x_{50\%}$=9, 4.5, and 3 mm, respectively, and all with x_o=0.3 mm. At x_{max}, instead of a sharp 90-degrees turn, in reality there is a smooth gradual transition as *F(x)* reaches 100% as shown by the dotted curve in Fig. 3a for the three examples. However, this does not affect high solids recovery in the 90 percentiles as required by the wastewater treatment plant as the behavior is dictated by the smaller particle sizes of the PSD curve.

Using the distribution profile Eq. 7a together with Eqs. 2b-d, the solids recovery can be shown after integrating Eq. 6 to take the following form,

$$R_s(x_c) = 2 + \frac{2}{ax_c}\exp(a(x_c - x_o)\left[-1 + \frac{1}{ax_c}\right] - \left\{\left(\frac{x_o}{x_c}\right)^2 - \frac{2}{ax_c}\left(\frac{x_o}{x_c}\right) + \frac{2}{(ax_c)^2}\right\} \tag{8}$$

2.3 Leung Number and Closed-form Solution

A dimensionless Leung number [4, 11], abbreviated *Le*, can be defined as follows

$$Le = \frac{\sqrt{Q/L}\sqrt{\mu/\Delta\rho}}{\Omega R_p x_{50\%}\eta_a} \tag{9}$$

Le number has been used successfully for scale-up for separation and classification of polydispersed size distribution using spin tubes [11] and continuous fed centrifuges, such as decanter [4] and disk stack centrifuges [10]. Most applications are for mineral processing with well-defined density and particle sizes [12], while certain well-defined biological solids in biopharmaceutial applications have been used as well [10]. The *Le* number embodies the

operating parameter (Q, Ω, η_a) and geometric variables (L, R_p) of the centrifuge together with the feed properties ($x_{50\%}$, μ, and $\Delta\rho$). It can be seen that the cut size x_c in Eq. 2d is related to Le via [4]

$$\frac{x_c}{x_{50\%}} = \frac{3}{\sqrt{\pi}} Le \tag{10}$$

Using the median size $x_{50\%}$ as a reference length dimension characterizing the feed flocs, the minimum floc size x_o, corresponding to the primary unflocculated particle, can be rendered dimensionless by,

$$\overline{x_o} = \frac{x_o}{x_{50\%}} \tag{11}$$

With Eqs. 10 and 11,

$$\frac{x_o}{x_c} = \left(\frac{x_o}{x_{50\%}}\right) \Big/ \left(\frac{x_c}{x_{50\%}}\right) = \frac{\sqrt{\pi}}{3} \frac{\overline{x_o}}{Le}$$

$$ax_c = \frac{cLe}{1-\overline{x_o}} \tag{12a, b, c}$$

$$c \equiv \frac{3}{\sqrt{\pi}} \ln(3/2)$$

Substituting Eqs. 12a, b into Eq. 8, the solids recovery becomes

$$R_s(x_c) = 2 + \frac{2\left(1-\overline{x_o}\right)}{cLe}\left[-1+\frac{1-\overline{x_o}}{cLe}\right]\exp\left\{\frac{cLe}{1-\overline{x_o}}\left[1-\frac{\sqrt{\pi}}{3}\frac{\overline{x_o}}{Le}\right]\right\}$$

$$-\frac{(\pi/9)}{Le^2}\left\{\left(\overline{x_o}\right)^2 - 2\overline{x_o}\left(\frac{1-\overline{x_o}}{\ln(3/2)}\right) + \frac{2(1-\overline{x_o})^2}{\left[\ln(3/2)\right]^2}\right\}; \quad Le \geq \frac{\sqrt{\pi}}{3}\overline{x_o} \tag{13a}$$

Eq. 13 is valid provided $x_c > x_o$ implying $Le \geq \frac{\sqrt{\pi}}{3}\overline{x_o}$ from Eq. 10. The result of the model thus can be expressed in terms of the two governing dimensionless parameters $\overline{x_o}$ and *Le*. While *Le* depends on the operating and geometric conditions of the decanter, fluid-particle properties, $\overline{x_o}$ depends on the feed and polymer flocculation. When these parameters are known solids recovery can be determined from Eq. 13a.

When the floc size becomes very large, or x_o becomes very small, $\overline{x_o} << 1$, Eq. 13a can be simplified to

$$R_s(x_c) \cong 2 + \frac{2}{cLe}\exp(cLe)\left[-1+\frac{1}{cLe}\right] - \left\{\frac{2}{(cLe)^2}\right\}, \quad \overline{x_o} << 1 \qquad (13b)$$

2.4 Buckingham-π analysis

It is of interest to examine the general dimensionless π groups that are important for separation in the moving layer using the Buckingham-π theorem; and compare the results to the dimensionless variables obtained from the analytical model developed in Sec. 2.2-2.3. The Buckingham-π analysis can be found in any standard fluid mechanics textbook; therefore, it is not repeated here except the analysis results. For a given clarifier design, there are a total of 11 variables that affect the settling of flocs in the moving layer. They are the feed rate *Q*, clarifier length L_c, pool radius R_p, bowl radius R_b, minimum floc size x_o, median floc size $x_{50\%}$, bowl rotation speed Ω, differential speed between conveyor and bowl $\Delta\Omega$, viscosity of suspension μ, density difference between floc and

suspension $\Delta\rho$, and suspension density ρ. Given these 11 variables are composed of three basic variables which are mass *M*, time *T*, and length *L*; therefore, there should be only 8 (=11-3) dimensionless π groups according to the Buckingham-π theorem. Three variables $\Delta\rho$, Ω, and R_p are chosen to form dimensionless groups with each of the 8 variables in turn. After making such analysis, the π groups are:

1) Rossby number

$$\pi_1 = \frac{Q}{\Omega R_p^3} = \frac{Q/R_p^2}{\Omega R_p} = \frac{u}{\Omega R_p} = Ro \qquad (14)$$

Rossby number measures relative velocity of the feed velocity to the absolute tangential speed of the pool surface. An estimate based on typical values reveals that $Ro < 0.1$.

2) Ratio of clarifier length-to-pool radius

$$\pi_2 = \frac{L_c}{R_p} \qquad (15)$$

The clarifier length-to-pool radius ratio is typically of orders of 10 based on configuration and operating of decanter and tubular centrifuges.

3) Ratio of clarifier bowl-to-pool radii

$$\pi_3 = \frac{R_b}{R_p} \qquad (16)$$

The clarifier bowl-to-pool radii ratio is typically about 2. Given flow occurs at the moving layer, this ratio may not have much influence unless R_b approaches R_p or R_b / R_p approaches unity for which the sediment on the bowl wall may affect the moving layer.

4) Ratio of minimum floc size to pool radius

$$\pi_4 = \frac{x_o}{R_p} \tag{17}$$

The minimum floc size to pool radius is very small.

5) Ratio of floc size to pool radius

$$\pi_5 = \frac{x_{50\%}}{R_p} \tag{18}$$

The median floc size to pool radius is very small.

6) Ratio of differential to bowl speed

$$\pi_6 = \frac{\Delta\Omega}{\Omega} \tag{19}$$

This ratio is important for cake conveyance. It is also important for sedimentation in the vicinity near the blade surface; however, given the distance between adjacent blades is usually much greater than the moving layer thickness, this effect should be negligible.

7) Modified Reynolds number

$$\pi_7 = \frac{\Delta\rho\Omega R_p^2}{\mu} = \frac{(\Delta\rho/\rho)\rho\Omega R_p^2}{\mu} \tag{20}$$

The modified Reynolds number is based on pool speed and density difference. This ratio is actually a product of a basic Reynolds number based on density $\frac{\rho\Omega R_p^2}{\mu}$ and the ratio of density difference to density $(\Delta\rho/\rho)$. It measures the inertia due to settling versus the viscous drag.

8) Density difference ratio

$$\pi_8 = \frac{\Delta\rho}{\rho} \tag{21}$$

This ratio is very small given the density difference between biological solids and the suspending liquid is small. As can be seen, this ratio has already been incorporated in the modified Reynolds number, so it becomes redundant. Indeed, other than the ratios $\pi_3 = R_b / R_p$ which have been considered not important unless the pool depth is comparable to that of the moving layer thickness, and one other π group ($\pi_8 = \frac{\Delta\rho}{\rho}$) becomes redundant, the remaining six π groups are all important. When comparing to the settling in surface moving layer, four π groups ($\pi_1, \pi_2, \pi_5, \pi_7$) out of the six can be combined into a more important π_9 group, which is the Leung number. Thus,

$$\pi_9 = \frac{1}{\pi_5}\left(\frac{\pi_1}{\pi_7 \pi_2}\right)^{1/2}$$

$$\pi_9 = \left(\frac{\pi_1}{\pi_7}\frac{1}{\pi_2}\frac{1}{\pi_5^2}\right)^{1/2} = \left(\frac{Ro}{\mathrm{Re}}\frac{R_p}{L_c}\left[\frac{R_p}{x_{50\%}}\right]^2\right)^{1/2} = \frac{\sqrt{Q/L}\sqrt{\mu/\Delta\rho}}{\Omega R_p x_{50\%}} \tag{22}$$

By squaring Eq. 22,

$$\left(\pi_9\right)^2 = \frac{2\pi Q}{\left(\frac{\Delta\rho x_{50\%}^2 (\Omega^2 R_p)}{\mu}\right)(2\pi L R_p)} = 2\pi\frac{Q}{v_s A_p} \sim Le^2 \tag{23}$$

Except for a constant 2π, the Leung number is essentially the square root of the ratio of the feed rate *Q* to the clarification rate by centrifugal sedimentation $v_s A_p$.

The Leung number is a combination of four dimensionless π groups (*Ro, Re, L_c/ Rp, x_{50}/R_p*).This is somewhat analogous to the Raleigh number used in natural convection, wherein $Ra = Gr\,\mathrm{Pr} = (\Delta\rho/\rho)\,\mathrm{Re}^2\,\mathrm{Pr}$. Thus, Ra is also a combination of three dimensionless π groups - the density difference ratio, Reynolds number, and the Prandtl number, *Pr*.

Returning to our analysis, similarly, $\pi_4 = \frac{x_o}{R_p}$ and $\pi_5 = \frac{x_{50\%}}{R_p}$ can be combined into a new dimensionless group,

$$\pi_{10} = \frac{x_o / R_p}{x_{50\%} / R_p} = \bar{x}_o$$

Now, π_9 and π_{10} are two important dimensionless variables (after re-combination) for the floc settling in the moving layer. These two new π groups, which are the direct consequence of the analytical model, involve the previous six π groups from the Buckingham-π analysis! As stated, the latter does not suggest which π groups are important for the problem and how they should be combined.

In summary, the results of the Buckingham-π analysis can also be re-grouped to derive *Le* and $\bar{x}_o$. These two dimensionless numbers actually involve all the basic dimensionless π groups with the exception of only one π group, R_b / R_p. In our model, there is also an accelerator efficiency η_a to account for the actual pool speed $V_t=\Omega R_p \eta_a$. The feed acceleration efficiency does not bear out from the Buckingham-π analysis given it is already dimensionless. However, the accelerator efficiency η_a can be incorporated into the denominator of Eq. 22 to

come up with identical form as Eq. 9. The above result is applicable to both decanter and tubular centrifuges [4, 8].

2.5 Model Solution

Fig. 3b shows the R_s plotted against *Le* corresponding to the assumed feed floc profiles of Fig. 3a. The Leung number is essentially the square root of the ratio of the feed rate to the clarification rate by centrifugal sedimentation. As *Le* increases R_s decreases for a fixed $\overline{x_o}$. As apparent from the definition of *Le* in Eq. 9, Le increases with

- increasing feed rate,
- decreasing clarifier length,
- higher suspension viscosity,
- smaller density difference,
- lower rotation speed,
- lower pool radius,
- smaller median floc size, and
- poorer feed acceleration efficiency.

On the other hand, for a fixed *Le* small $\overline{x_o}$ gives lower R_s (the limit being $\overline{x_o}$=0 corresponding to the bottom curve in Fig. 3b, see Eq. 13b), vice versa for large $\overline{x_o}$ that gives higher R_s.

These theoretical results will be deployed for predicting the floc sizes and solids recovery subsequently.

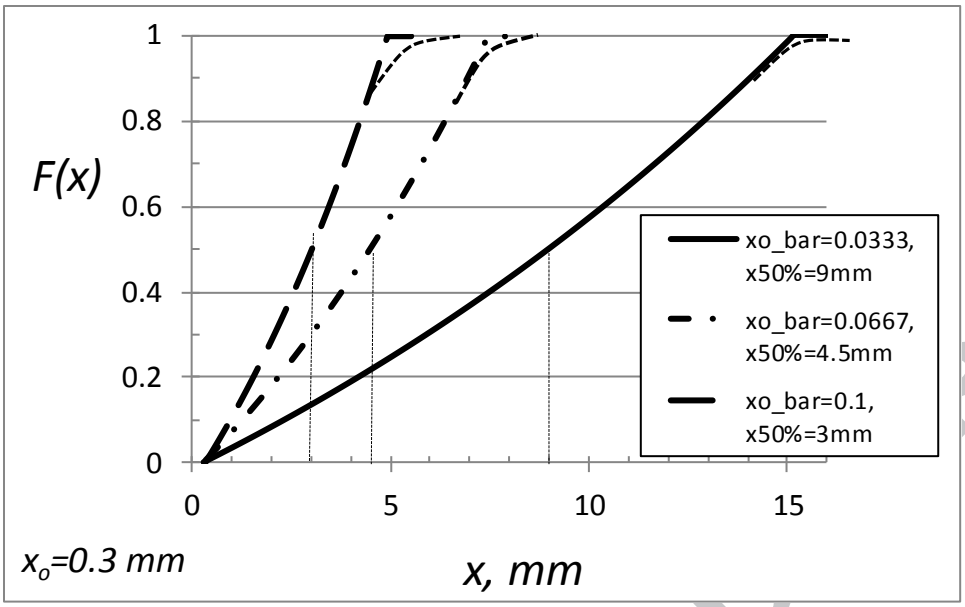

Fig. 3a – Three feed size distributions with $x_{50\%}$=9, 4.5, and 3 mm all with x_o=0.3mm, corresponding to $\overline{x_o}$ =0.033, 0.067, and 0.1, respectively.

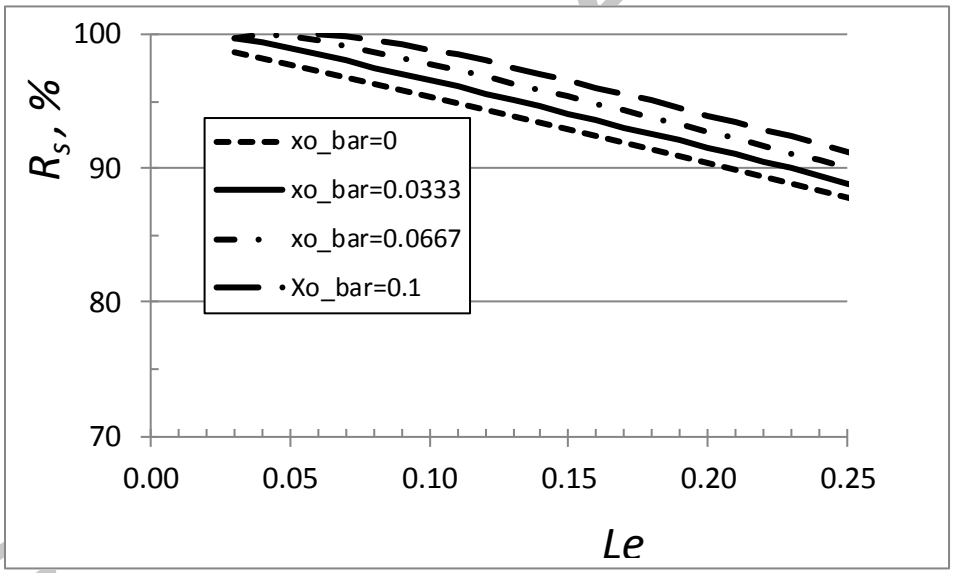

Fig. 3b – Solids recovery as function of *Le* and $\overline{x_o}$ with feed floc size distribution in form given by Eqs. 7a, b.

3. Field Test

Two continuous-feed decanter centrifuges were deployed for carrying out field tests in a wastewater treatment plant that processed a mixed sludge with 52% waste activated sludge from secondary treatment and 48% primary sludge from primary treatment. The cake solids have dry matter content between 29-30% [13]. A polymer solution was prepared from dissolving Percol 789 polymer (powder) in deionized water to produce a solution with concentration of about 0.3%. One machine HS has diameter 427 mm by length 1372 mm for which operating parameters were varied for testing purposes, while the smaller machine DS has diameter 429 mm by length 1257 mm and was run at fixed condition as a reference machine. When feed sludge properties changed during the day, they affected both machines and a fair comparison could be made between the two machines.

The feed solids concentration was about 5% by weight. In the tests, the feed rate, pool level, polymer dosage for the HS decanter were changed. Differential speed between the screw conveyor and the bowl was adjusted to reduce the torque and was typically at 5 rev/min or less [14]. The test conditions are compiled in Table 1. After steady-state has been reached, the samples from the feed, centrate and cake were taken at least in duplicate (for averaging purposes). The samples were dried in an oven overnight at which the solids concentration for the sample was determined by gravimetric analysis. Based on the solids concentration (by dry weight basis) in the feed W_f, centrate W_e, and cake W_s, the solids recovery R_s can be calculated from material balance [4]

$$R_s = \frac{1 - W_e / W_f}{1 - W_e / W_s} \tag{15}$$

Table 1 – Machine settings and conditions

Decanter Centrifuge	Test Series	Pool setting (radius, mm)	rev/min (G)	Q, m^3/h
HS	062294	463 (111.13)	3125 (2500g)	8.6-12.2
HS	062894			6.1-15.0
HS	062994	475 (107.95)		6.1-15.0
DS	062894, 062994	400 (113.03)	3300 (2600g)	10.0-10.5

By way of example, Fig. 4 shows solids recovery for three sets of field data (23 tests) collected for the HS decanter. First, the solids recovery decreases with increasing feed rate. This is due to less retention time for the flocs to settle in the moving layer. Second, the recovery is reduced with a shallower pool because of poorer feed acceleration as discussed in sec. 1.3.

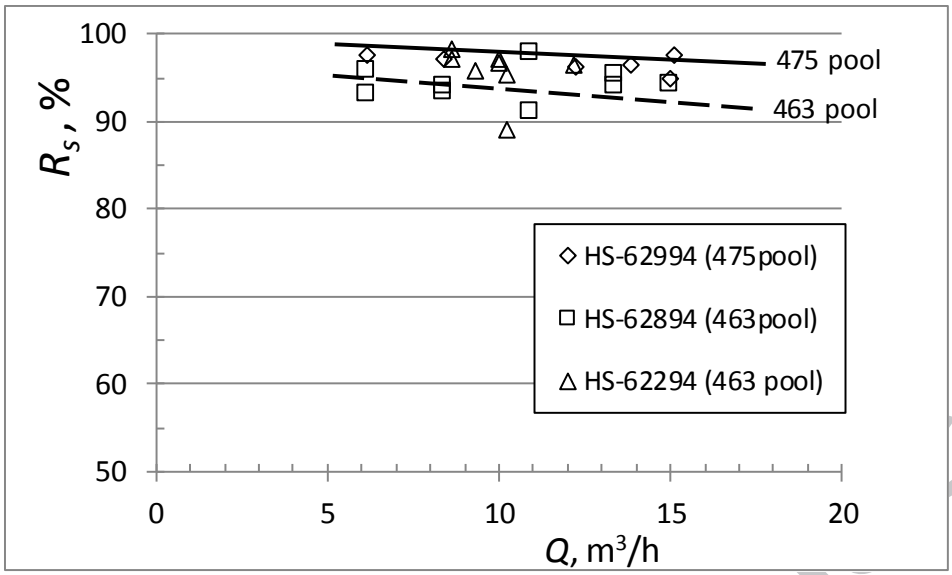

Fig. 4 – Solids recovery versus feed rate for two different operating pool levels 463 pool and 475 pool setting. The bowl speed was at 3125 rev/min.

4. Determining in-situ floc size

4.1 Leung number calculation

Given the Leung number is used in the analysis throughout, it is useful to illustrate the calculation by way of an example, which is an excerpt from a test from Series HS-062994:

Q=13.85m^3/h, L=1.2m, $\mu/\Delta\rho$=3000 cm^2/s, $x_{50\%}$=10 mm, Ω=3125RPM,

R_p=107.95mm, R_a=101.6mm, R_s=96.4%.

(Note $x_{50\%}$=10 mm is an assumed value for the initial matching with the test data.)

$$Le = \frac{\sqrt{Q/L}\sqrt{\mu/\Delta\rho}}{\Omega R_p x_{50\%}\eta_a} = \frac{\sqrt{(13.85/3600)/1.2}\sqrt{3000(10^{-4})}}{[(3125)\pi/30](0.107)(0.01)(0.5)(1+\left[\frac{0.102}{0.107}\right]^2)}$$

$$= \underline{0.0931}$$

In the above, the efficiency of the feed as it enters the pool is given by $(R_a/R_p)^2$ [4]. Any efficiency that differs from 100% (i.e. less than 100% representing under-acceleration, and greater than 100% representing over-acceleration) would lead to mismatch of the incoming feed with the rotating pool speed causing turbulence with consequence of breaking delicate flocs to smaller sizes. However, as the feed travels downstream in the clarifier, it would eventually accelerate to 100% by contact with the pool liquid under solid-body rotation, therefore, the overall feed acceleration efficiency in the clarifier is taken as an average between these two limits in the above calculation.

4.2 Matching data to model prediction

First, the *Le* number was calculated as shown for all test data assuming $x_{50\%}$=10mm. This also defines $\overline{x_o} = 0.3mm/10mm = 0.03$ and a Rs-prediction curve was generated between the minimal value *Le* (=$\left(\sqrt{3}/\pi\right)\overline{x_o}$) and the maximum, say *Le*=0.25, for $\overline{x_o} = 0.03$ using Eq. 13a. The prediction R_s-curve generated was compared with the test data in the same R_s - *Le* plot. If the two did not match, another $x_{50\%}$ was assumed and the calculations was repeated until the test data and the prediction match up. Typically, only a few iterations sufficed for the matching process.

Fig. 5a compares the solids recovery prediction curves (solid and broken lines) and the field test data (symbols) for the three different trial values of $\overline{x_o}$ =0.06, 0.03 and 0.02 that correspond to $x_{50\%}$=5, 10, 15 mm, respectively, with x_o=0.3 mm. The test data was from test HS-062994 with the decanter operating at 475 pool setting. In Fig. 5a, only $\overline{x_o}$ =0.03 provides a closer match between the solid recovery prediction and the test data. Fig. 5b shows the refinement match between the model prediction and the test data after a few iterations. The solids prediction curve with $\overline{x_o}$ =0.0357 (x_o=0.3 mm and $x_{50\%}$ of 8.41mm) has the best match with the test results.

On the other hand, Fig. 6 shows the best match between the model prediction with the test HS-062294 with the decanter operating at 463 pool setting. Again, the *Le* number was calculated for all the test data and plotted on Fig. 6 to overlay with the theoretical prediction curves. The curve, that has $\overline{x_o}$ =0.0625, corresponding to $x_{50\%}$=4.8mm, has the best match with the test data.

Finally, Fig. 7 shows the best match between the model prediction with the test series 062894 and 062994 obtained from a second decanter DS, which was operated at 400 pool setting and much higher angular speed. Again, the *Le* number was calculated for all the test data and plotted on Fig. 7 to overlay with the theoretical prediction curves. The curve, that has $\overline{x_o}$ =0.0559 corresponding to $x_{50\%}$=5.37mm, has the best match with the test results. Indeed, this $x_{50\%}$ value is not too far off from that obtained from the HS-062294 test conducted with the larger decanter.

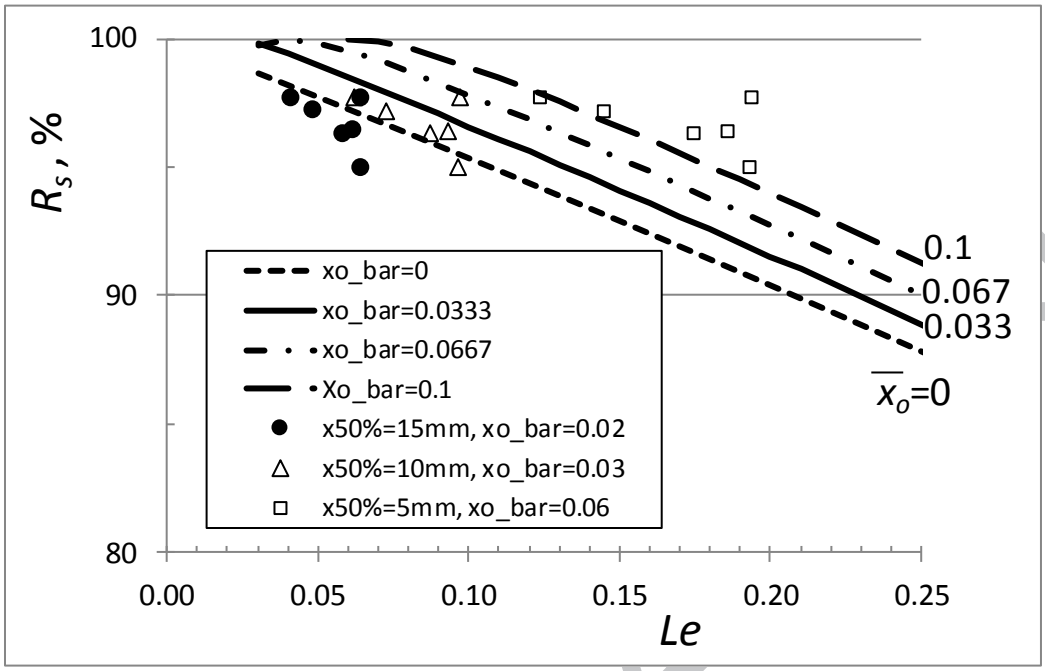

Fig. 5a – Three different trials of predictions matching with field test data assuming $\overline{x_o}$ =0.06, 0.03 and 0.02 corresponding to respectively $x_{50\%}$=5, 10, 15 mm. The data was from HS-062994 with 475 pool setting.

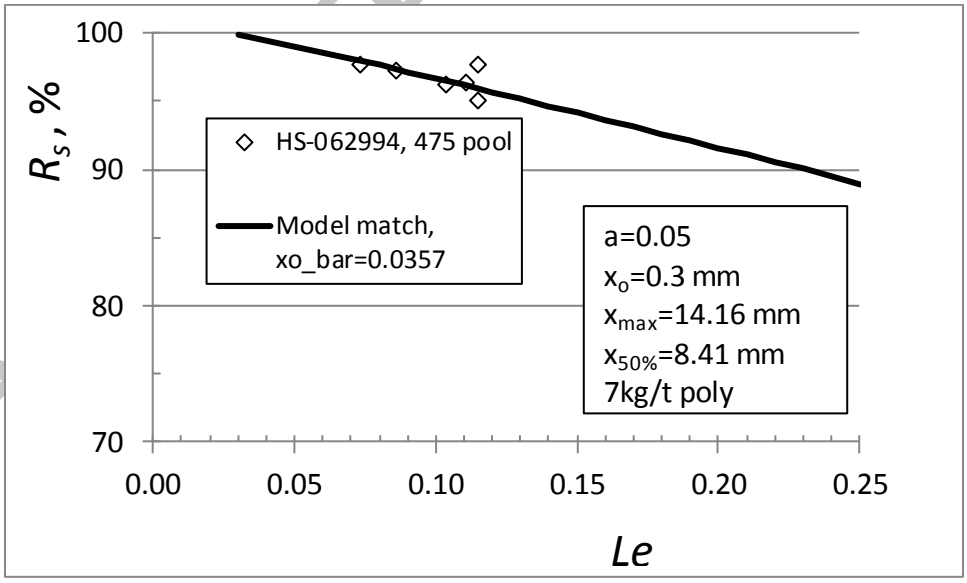

Fig. 5b – Matching of solids recovery between test data for HS – 062994 at 475 pool setting and model prediction. The match results indicate $\overline{x_o}$ =0.0357 and $x_{50\%}$=8.41 mm given x_o=0.3 mm.

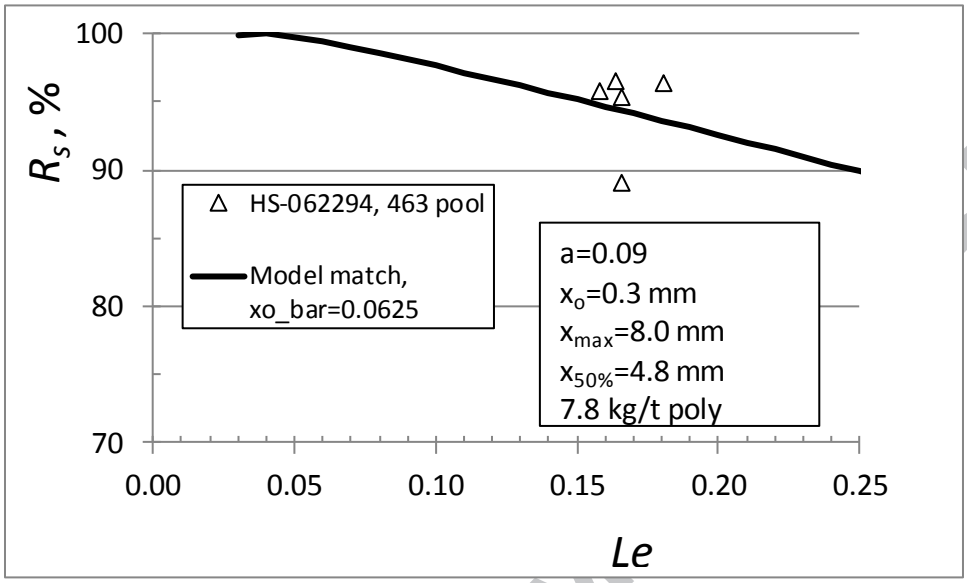

Fig. 6 – Matching of solids recovery between test data for HS – 062294 at 463 pool setting and model prediction. The match results indicate $\overline{x_o}$ =0.0625 and $x_{50\%}$=4.8 mm given x_o=0.3 mm.

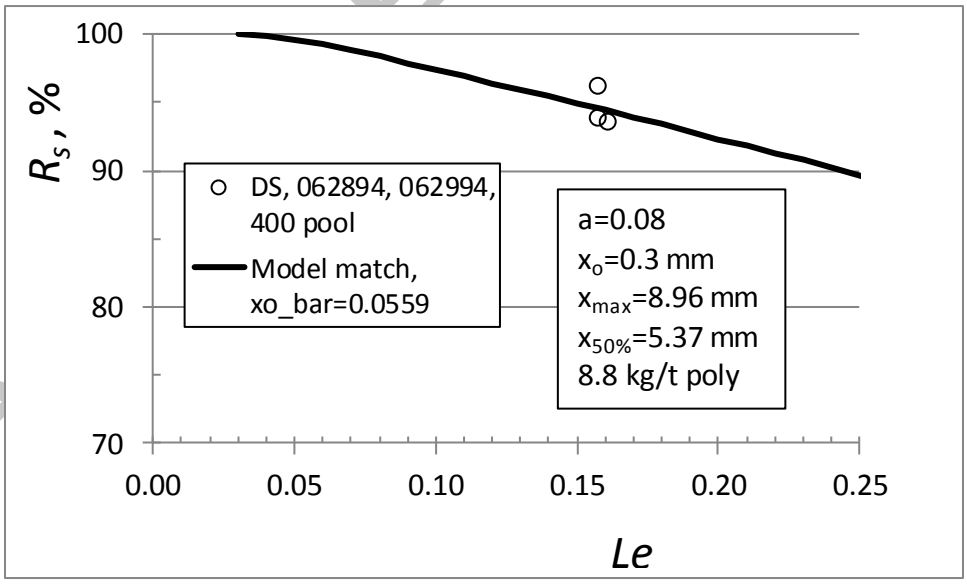

Fig. 7 – Matching of solids recovery between test data for DS – 062894 and 062994 at 400 pool setting and model prediction. The match results indicate $\overline{x_o}$ =0.0559 and $x_{50\%}$=5,37 mm given x_o=0.3 mm.

The three sets of data on the inferred in-situ floc size are summarized in Table 2. At this point, it is appropriate to interpret the results to ensure that they are meaningful. Also, the loss in acceleration efficiency due to the feed accelerator discharge radius being smaller than the larger pool radius can be estimated from [4]

$$\eta = \left(\frac{R_a}{R_p} \right)^2 \eta_a \qquad (15)$$

The results are shown in Table 2. The polymer dosage from field tests is also compiled in the same table.

For the HS-062994 at 475 pool, given the deeper pool setting, the efficiency as determined from Eq. 15 is the highest at 89%. There is less disturbance of the floc as it is laid gently on the pool surface. Consequently, the amount of polymer consumed is the least among all, at 7 kg/t, and the floc is the largest due to less shear and turbulence. In actuality, at high feed rate there is a dynamic liquid head, which brings the pool even deeper and closer to the discharge radius of the feed accelerator rendering closer matching with even less disturbance in the pool at the feed entry point. Therefore, the above is a very conservative estimate, yet it illustrates the point.

In contrast, for the HS-062294 at 463 pool, given the shallower pool setting, the efficiency is only 84%. There is more pool disturbance and consequently more

breakage of the flocs as the flocculated feed is laid onto the pool. This case consumes 8.3kg/t polymer which represents 19% more polymer consumption to maintain floc integrity, otherwise recovery would have been plunged down to an unacceptable level below 90%. In conjunction, the floc size has also been reduced to 4.8 mm, which is 43% reduction in size compared to the 475 pool setting.

Finally, for the smaller decanter DS-062894 and DS-062994 at 400 pool, given the shallower pool setting, the efficiency is only 80%. There is much more disturbance of the pool during feed entry resulting in breakage of the flocs to smaller sizes. Indeed, the floc size reduces to 5.3mm which is much smaller when compared to 8.4mm from the HS-062994. This represents a 36% reduction as compared to the HS-062994 operating at a deeper pool! Further, a higher polymer dose of 8.8 kg/t (which is 26% in excess of the HS-062994 at 7 kg/t) is required to maintain the flocs from breakage.

Overall, higher feed acceleration efficiency (89%) results in larger flocs ($x_{50\%}$=8.4 mm) and lower polymer dosage (7kg polymer/ton sludge); while poorer feed acceleration efficiency (80%) results in smaller flocs ($x_{50\%}$=8.4 mm) and higher polymer dosage (8.8kg/t). Indeed, the inferred floc size fits very nicely into the explanation on feed acceleration efficiency and polymer consumption from field tests.

Table 2 – Pool depth, efficiency, polymer dose and median floc size in-situ

decanter	Series	Pool	Efficiency at pool	kg/t	$x_{50\%}$, mm
HS	62294	463	84%	8.3	4.8
HS	62994	475	89%	7	8.4
DS	062894/062994	398	80%	8.8	5.3

5. Prediction

One can use Eq. 13a to predict solids recovery for decanter centrifuge operation. Assuming the median floc size $x_{50\%}$ = 4.8 mm at 463 pool and x_o=0.3 mm, the model prediction is compared with the field tests HS-062894 in Fig. 8. As can be seen, despite some scatter in the test data the comparison is reasonable confirming that the model can play an important role in predicting the solids recovery in a decanter.

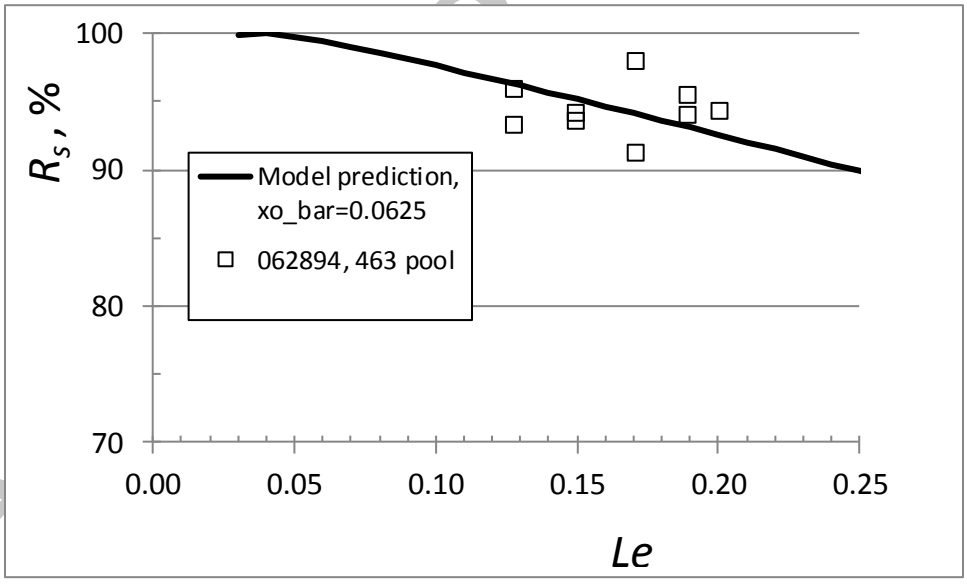

Fig. 8 – Comparing solids recovery prediction with test data for HS – 062894 at 463 pool setting (assumed $\overline{x_o}$ =0.0625 and $x_{50\%}$ = 4.8 mm).

6. Scale-up

Finally, all four sets of data are plotted against the Leung number assuming an average of $\overline{x_o}$ =0.05 (i.e. average of $\overline{x_o}$ =0.0359, 0.0559, 0.0625) with $x_{50\%}$ = 6 mm and x_o=0.3 mm. Despite small variation in the test data, they are reasonably correlated by the prediction. This is a rather remarkable result for scale-up of two machines of different designs, sizes, and operating conditions. In the past, most of the field test data are typically plotted in form of Fig. 4 that are of limited use. For a given sludge, identical machine designs with different sizes provide test data that are difficult to be scaled-up [4], let alone test data obtained for which the designs of the centrifuges are different. In comparison with the past, the present approach has already made a big leap forward!

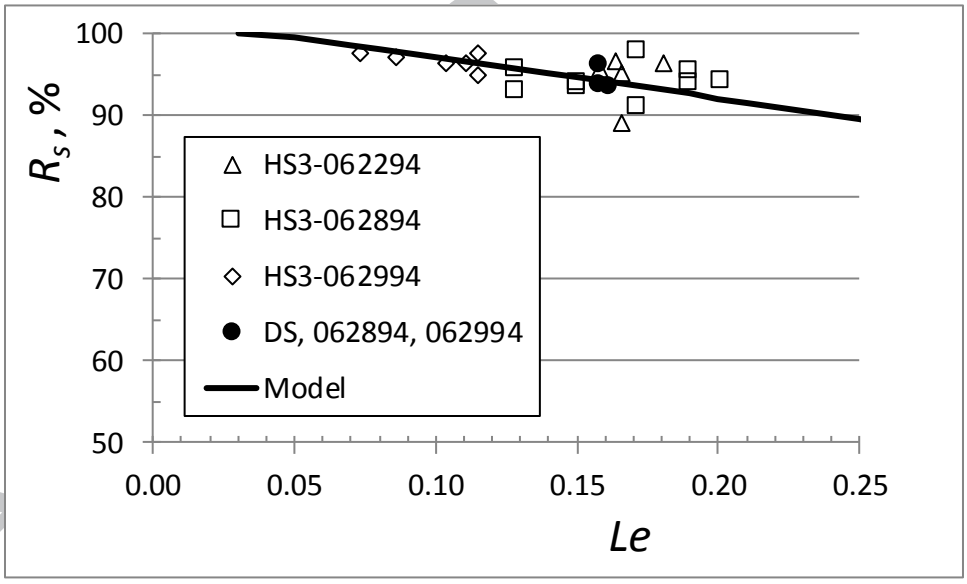

Fig. 9 – Solids recovery versus Leung number for all test data assuming an average of $\overline{x_o}$ =0.05 for all four sets of tests.

7. Conclusions

The moving layer for continuous-feed centrifuge with large length-to-diameter aspect ratio has been confirmed independently by flow visualization using fluorescent dye and by conductivity measurement. A model on sedimentation of flocs in the moving layer has been developed. Using an exponential curve for the floc PSD, the solids recovery can be expressed explicitly in analytical form in terms of the dimensionless Leung number and the minimum-to-median floc size ratio. A rigorous Buckingham-π analysis also confirms these two dimensionless number and ratio. Four sets of test runs, encompassing a total of over 20 field tests in a secondary wastewater treatment plant, have been carried out on sedimentation of flocculated mixed sludge in two decanters of different sizes, designs and operating conditions.

Based on the model and test results, the present approach can infer the in-situ floc size, which may be much smaller than that of the jar tests. Given the solids recovery is determined by settling which critically hinges on the floc size, this explains the incorrect scale-up reported in the past largely due to un-detected floc size attrition from turbulence and shear, especially with poor feed acceleration.

One important application is that when the floc size is known or can be estimated, useful prediction can be made on the solids recovery of the decanter.

Finally, the Leung-number approach offers help in scale-up not only on well-defined minerals with known density, such as minerals, but also on flocculated biological solids as demonstrated in this study. This opens up a new window of opportunity for other applications.

Nomenclature

a coefficient in Eq. 7a, m^{-1}

A_p pool area, m^2

c coefficient in Eq. 12c

G centrifugal gravity, m/s^2

Gr *Grashof number, [-]*

h height or thickness of moving layer, m

L, L_c clarifier length, m

Le Length number, [-]

Pr *Prandtl number, [-]*

Q feed rate, m^3/s

Ra *Raleigh number, [-]*

R_a accelerator feed port radius, m

R_b bowl radius, m

Re Reynolds number, [-]

R_p pool radius, m

R_s solids recovery, %

Ro Rossby number, [-]

S streamflow distance, m

t_R *retention time, s*

u throughflow velocity, m/s

v_s settling velocity, m/s

W_e centrate solids concentration, %w/w

W_f feed solids concentration, %w/w

W_s cake solids concentration, %w/w

x_o minimum floc size, m

x_c cut size, m

$x_{50\%}$ median floc size, m

$\bar{x}_o$ $x_o/x_{50\%}$, [-]

y vertical distance, m

y_c vertical distance for the critical trajectory, m

z removal fraction, [-]

Vectors

ba' tangential speed of feed assuming it is at solid-body rotation ΩR_a

b'a' tangential speed of feed after free-flight to larger pool radius R_p

bb' radial velocity induced after feed free-flight to larger pool radius R_p

ba tangential speed of pool under solid-body rotation ΩR_p

Greek Symbols

$\Delta\rho$ density difference, kg/m^3

ρ suspension density, kg/m^3

μ viscosity, kg/m-s

ν kinematic viscosity, m^2/s

π dimensionless group, [-]

η efficiency, %

Ω rotation speed of bowl, rad/s

$\Delta\Omega$ differential rotation speed between bowl and conveyor, rad/s

Acknowledgement

The author is grateful to Professor Ascher H. Shapiro, late Institute Professor of MIT, for his valuable suggestion.

References:

[1] G.M. Fair, J.C. Geyer, D.A. Okun, Water and wastewater engineering, vol. 1 & 2, John Wiley and Sons, New York, (1967).

[2] J. Gregory, The action of polymeric flocculants, ed. B.M. Moudgil and P. Somasundaran, Pro. of Eng. Found. Conf., Sea Island, GA, (1985) 125-137.

[3] E.A. López-Maldonadoa, M.T. Oropeza-Guzman, J.L. Jurado-Baizavala, A. Ochoa-Terán, Coagulation–flocculation mechanisms in wastewater treatment plants through zeta potential measurements, J. Haz. Mat., 279 (2014), 1-10.

[4] W.W.F. Leung, Industrial Centrifugation Technology, McGraw-Hill, New York, (1998).

[5] W.W.F. Leung, Centrifuges, Perry & Green Chemical Engineers' Handbook, D. Green (editor), 7th ed., McGraw-Hill, New York (1997), 18, 106-125.

[6] ASTM D2035-13, Standard Practice for Coagulation-Flocculation Jar Test of Water, ASTM International, West Conshohocken, PA, 2013.

[7] Y.H. Kim, J.P. Hsu, Characterization of Turbulence-Induced Aggregate Breakage, ed. B.M. Moudgil and P. Somasundaran, Pro. of Eng. Found. Conf., Sea Island, GA, (1985) 191-204.

[8] W.W.F. Leung, A.H. Shapiro, Efficient double-disc accelerator for continuous-feed centrifuges, Filtration and Separation, Oct 1996, pp 819.

[9] W.W.F. Leung, A.H. Shapiro, Feed Accelerator System Including Accelerator Vane Apparatus, United States Patents 5,520,605, May 1996, and United States Patents 5,551,943, Sept. 1996

[10] W.W.F. Leung, Centrifugal Separation in Biotechnology, Academic Press-Elsevier, Oxford (2007).

[11] W.W.F. Leung, Separation of Dispersed Suspension in Rotating Tube, Sep. & Puri. Tech., 38 (2004), 99-119.

[12] W.W.F. Leung, Centrifugal Separation, Plant Design Handbook for Mineral Processing, Proc. Minerals Processing Plant Design, Practice, and

Control, ed. A. Mular, D. Halbe, and D. Barratt, Soc. Min. Eng. (2002), 1262-1288.

[13] W.W.F. Leung, R Havrin, High-Solids Decanter, Fluid Particle Separation, J., 5, #1 (1991).

[14] W.W.F. Leung, Torque Requirement for High-Solids Centrifugal Sludge Dewatering, Filtration and Separation, (1998), 882-887.

Highlights

- Determine in-situ floc size by matching model and test results
- Model predicts solids recovery using Leung number and floc size ratio
- Scale-up decanters for separating floc suspension
- Field tests on mixed sludge using 2 decanters